Available online at www.sciencedirect.com
SCIENCE DIRECT®
Journal of Magnetic Resonance 162 (2003) 259–268
JMR Journal of Magnetic Resonance
www.elsevier.com/locate/jmr

Automated data processing of {^{1}H-decoupled} ^{13}C MR spectra acquired from human brain in vivo

Frederick Shic[a] and Brian Ross[b,*]

[a] *Rudi Schulte Research Institute, Santa Barbara, CA, USA*
[b] *MR Spectroscopy Unit, Huntington Medical Research Institutes, 660 S. Fair Oaks Ave, Pasadena, CA 91105, USA*

Received 17 September 2002; revised 28 March 2003

Abstract

In clinical ^{13}C infusion studies, broadband excitation of 200 ppm of the human brain yields ^{13}C MR spectra with a time resolution of 2–5 min and generates up to 2000 metabolite peaks over 2 h. We describe a fast, automated, observer-independent technique for processing {^{1}H-decoupled} ^{13}C spectra. Quantified ^{13}C spectroscopic signals, before and after the administration of [1-^{13}C]glucose and/or [1-^{13}C]acetate in human subjects are determined. Stepwise improvements of data processing are illustrated by examples of normal and pathological results. Variation in analysis of individual ^{13}C resonances ranged between 2 and 14%. Using this method it is possible to reliably identify subtle metabolic effects of brain disease including Alzheimer's disease and epilepsy.

Keywords: ^{13}C; In vivo human brain; Glutamate; Neuron; Spectroscopy processing; Glia; Alzheimer; Epilepsy; Ketogenic diet

1. Introduction

^{13}C NMR (MRS), one of the most powerful of analytical tools in chemistry, has had limited impact in biomedical MR. Limitations of ^{13}C MRS in vivo include hardware demands of stable broadband excitation and of a second RF channel for proton decoupling, the low natural abundance of ^{13}C (1.1%), and the low signal-to-noise of the carbon nucleus as well as the cost and limited availability of appropriate ^{13}C enriched precursors. Despite all of these apparent drawbacks, a number of investigators have demonstrated the feasibility of in vivo ^{13}C MRS [1–4] and made important discoveries concerning normal brain metabolism [5–7]. Widespread use of ^{13}C MRS of humans is now predicted.

The direct demonstration of elements of the neurotransmitter events around the glutamine–glutamate cycle [8] is central to the understanding of normal and abnormal human brain metabolism. Because glutamate neurotoxicity is believed to underlie many different diseases, including epilepsy, Huntington's Disease, stroke, and amyotrophic lateral sclerosis (Lou Gherig Disease) [9], ^{13}C MRS has begun to demonstrate widespread clinical and research utility. Rationalization of intravenous and oral infusion protocols has allowed significant numbers of patients [10], including infants [4], to be examined after enrichment of brain metabolites with [1-^{13}C]glucose, [1-^{13}C]acetate [6,11], or [2-^{13}C]acetate [12].

Direct ^{13}C MR detection after broadband excitation of 4 kHz and decoupling bandwidth 640 Hz allows characterization of at least 37 ^{13}C resonances, including the infused substrate and the final product of its intracerebral oxidation, bicarbonate (HCO_3^-), every 2–5 min. Thus, in a typical human brain study lasting 200+ min after exogenous ^{13}C enrichment, over 2000 peaks must be identified, quantified, and compared. So rapid has been the expansion of in vivo human ^{13}C MRS at 1.5 T that its use is now limited, not by scanner time, isotope cost or the availability and consent of patients, but by the monumental task of ^{13}C data processing.

For complete metabolic analysis of a modern ^{13}C infusion MRS study three approaches are currently being explored.

1. *Dynamic metabolic analysis (DMA)*: In vivo modeling of flux rates using known biochemical pathways and enzyme activity known as dynamic metabolic analysis (DMA), a direct extension of radioactive flux

* Corresponding author. Fax: 1-626-397-5846.
E-mail address: mrs@hmri.org (B. Ross).

1090-7807/03/$ - see front matter © 2003 Elsevier Science (USA). All rights reserved.
doi:10.1016/S1090-7807(03)00117-4

measurements with ^{14}C, has been the primary method of ^{13}C data analysis in published papers [2] and references therein.

2. *Isotopomer analysis (ITP)*: Detection of the multiplets which arise from *J*-coupling between the five carbon-atoms of glutamate, for example allows so-called Isotopomer analysis (ITP). In principle, ITP, by providing $2^5 = 32$ isotopomers [13], must illuminate more about glutamate in human brain function. With broadband excitation, all five of the carbon atoms of glutamate and glutamine can be followed over time in the same individual, providing unique insight into astrocyte-neuronal interactions that underlie the glutamate–glutamine cycle.
3. *Dynamic difference spectroscopy (DDS)*: In practice, pattern recognition of the evolving ^{13}C spectra has proven to be the simplest approach. After construction of robust difference spectra (DDS), the time to first appearance, the time constants of appearance and disappearance of commonly observed metabolites, ratios of metabolic enrichment in relation to other observable metabolites, and the early detection of ^{13}C in unexpected metabolites in a given patient are compared to the ^{13}C profile of a group of normal controls [10].

All three methods are dependent on accurate analysis of large numbers of spectra. Analysis of as many metabolites as possible, including molecules enriched but not necessarily implicated in the metabolic pathways under consideration, strengthens the interpretation of dynamic metabolic data acquired from human ^{13}C MRS studies [7]. Rapid data processing of large numbers of peaks simultaneously is essential if clinical use is to be made of the results of 13C MRS studies. Data would then become available in the same time frame as other diagnostic tests, including blood work. Automation is indispensable and minimizes user-dependent error. In this paper, we describe an observer-independent technique for the automatic pre-processing of {^{1}H-decoupled} ^{13}C directly detected spectroscopic signals in human brain spectra after the administration of [1-^{13}C]glucose and/or [1-^{13}C]acetate. Examples of normal and pathological results are shown to illustrate the techniques addressed.

A preliminary report of this work was presented [11,24].

2. Patients and methods

Normal volunteers ($N = 10$) and patients ($N = 20$) attending for diagnostic MRI and ^1H MRS, were selected for examination by ^{13}C MRS after appropriate ^{13}C-substrate infusions. The precise details are given in prior published papers [6,10,11,14]. Informed consent of each subject, IRB approval and, where applicable FDA approval under IND 56,510 or 59,950 were obtained.

2.1. Data acquisition

The data used in analysis were acquired on a 1.5 T GE clinical broadband MR scanner equipped with a second channel for proton decoupling. A doubly tuned surface coil was used for localization, MRI, ^1H MRS and the acquisition of {^{1}H decoupled} (640 Hz, WALTZ-16) ^{13}C spectra (4 kHz excitation, 5 kHz reception, 1024 complex data points) as described in [14–16]. Since ^{13}C spectra were acquired without further localization, glycerol and lipid peaks arising from interposed scalp and bone-marrow were also identified.

2.2. Data preparation

For the preparation of pulse-and-acquire data, all data was appropriately time-shifted to account for acquisition delay and zero-filled to a standard length (8192 complex points). No apodization was applied.

2.3. Correlation of spectra

The MR scanner is subject to instability due to B_0 variation which induces frequency shifts, coil heating which changes decoupling and excitation power, and several sources causing small deviations in phasing. To compensate for these effects, we corrected spectra in relation to reference spectra.

2.3.1. Reference spectra

In each experiment, a reference spectrum was constructed from 20 min of pre-infusion scans and subject to manual zero-order phasing. The reference was frequency shifted to a standard chemical shift by first identifying the half-max center frequency (HMCF) of the major methylene component using the following search method (Fig. 1). This method was effective because it alleviates errors in the imprecise location of maxima in non- symmetric or non-Lorentzian peaks and problems associated with fitting, including systematic drift, phasing problems and overlapping metabolites:

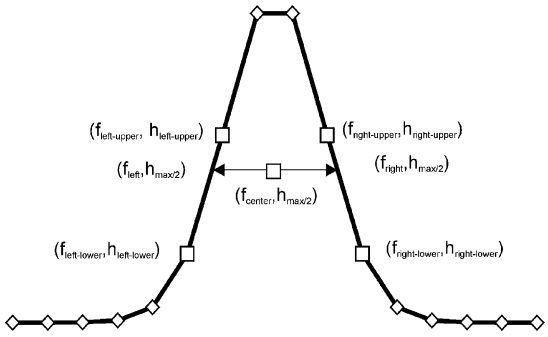

Fig. 1. Estimation of half maximum center frequency (HMCF). For frequency shifting of the reference spectrum, HMCF was first established, as described in text, followed by manual phasing.

(a) The magnitude of the reference signal is taken.
(b) The major component of methylenes is identified by a simple maximal search to get the frequency $f_{\max}$ and height $h_{\max}$.
(c) Iterate to the left for each point $(f_{\text{left-lower}}, h_{\text{left-lower}})$ until $h_{\text{left-lower}} < (h_{\max}/2)$. Step back once to the right to get the point $(f_{\text{left-upper}}, h_{\text{left-upper}})$. Then use linear interpolation to obtain a good estimate for f_{left} (with $h_{\text{left}} = h_{\text{right}} = h_{\max}/2$):

$$f_{\text{left}} = [(h_{\text{left}} - h_{\text{left-lower}})/(h_{\text{left-upper}} - h_{\text{left-lower}})] \times (f_{\text{left-upper}} - f_{\text{left-lower}}) + f_{\text{left-lower}}.$$

(d) Similarly compute for the right-hand side:

$$f_{\text{right}} = [(h_{\text{right-upper}} - h_{\text{right}})/(h_{\text{right-upper}} - h_{\text{right-lower}})] \times (f_{\text{right-lower}} - f_{\text{right-upper}}) + f_{\text{right-upper}}.$$

(e) Compute $f_{\text{center}} = (f_{\text{right}} + f_{\text{left}})/2$.

The frequency shift applied to the reference spectra was then calculated by subtracting f_{center} from a standard frequency (30.5 ppm) in order to match the chemical shifts as reported in [16]. This method for frequency determination, in comparison to a simple maximum search, reduced variation by over 95%. Frequency shifting was accompanied by an appropriate zero-order phase change in order to account for the interaction between the time shift of first-order phasing and frequency shifting.

2.3.2. Parameter estimation for reference matching

Each spectrum in the infusion study was matched to the reference spectrum by correcting for three sources of variation: frequency shift (f), zero-order phase change (ϕ), and global scaling (s). To obtain an estimate of these parameters we assumed spectrum F was to be matched to reference spectrum G and that F and G were related by:

$$F(t) = sG(t)e^{i(2\pi ft+\phi)}.$$

Dividing $G(t)$ by $F(t)$ gave the translation function $H(t)$:

$$H(t) = s^{-1}e^{-i(2\pi ft+\phi)}.$$

The scale that needed to be applied to $F(t)$ was determined by taking $\|H(0)\|$, the phase by $(\tan^{-1}(\text{Im}\{H(0)\}/\text{Re}\{H(0)\}))$, and the frequency by the Fourier transform of $H(t)$ after 4 Hz exponential apodization using the HMCF search algorithm described previously.

2.3.3. Fine-tuning of parameter estimation

The final step in the correlation of spectra was fine-tuning through iterative search:

(a) *Frequency shifts*: Given the initial estimates of frequency shift f_0 it is then possible to iterate over small deltas Δf in order to determine the shift that will minimize an error metric based on the differences of the magnitude of spectra, using the following algorithm: scan the delta frequency range R_i ($R_0 = 10$ Hz) with N steps ($N = 10$ steps) to find the frequency Δf_i that minimizes the error E_i, then set up a new frequency range $R_{i+1} = \{\Delta f_i \pm R_i/(N-1)\}$ and repeat (a) M times ($M = 10$ iterations).
(b) *Phase changes*: Zero-order phase changes can be corrected for in the same manner ($M = 10$ iterations).
(c) *Scaling changes*: Coil heating may result in a gradual loss of both transmitter and decoupling power. The determination of a scaling factor to once again minimize an error metric as applied to the magnitude spectra can be used to partially account for these signal losses. ($M = 8$ iterations).

Fine-tuning improved reference matching by 16.3% as measured by absolute difference for a group of patients ($N = 11$) versus a single reference control. The use of more advanced methods of multi-dimensional search, such as downhill simplex [17], did not significantly affect the simulation.

2.3.4. Choice of metric for fine-tuning

The choice of an error metric is important to the proper determination of "best parameter" choice. All metrics were comparable: [Variance, 57.189 dB; Absolute deviation, 57.186 dB; Lorentzian, 57.107 dB; and Pearson VII, 57.107 dB], but employing variance as an error metric lead to the highest signal-to-noise ratio.

2.3.5. Complete correlation routine

To summarize, first a reference spectrum was created. Subsequent spectra were frequency shifted using the HMCF search. Parameter estimation for reference matching was then applied to the new spectra, and if this reduced the error as measured by variance, the parameter estimation was accepted. HMCF search alone was sufficient for matching spectra in close temporal proximity, whereas parameter estimation was necessary for widely varying spectra. Three iterations of *fine-tuning* were applied in either case. No set of spectra needed more than one pass of this procedure. Typically, repeated application of this procedure resulted in a change of less than 2%. Each application took 8.0 s ($N = 10$) to complete on custom software written in IDL on a Sparc Ultra 10. Thus, for a patient examination of 200 min, data processing could be completed within 5 min. The improvements in spectral averaging in a single patient with Alzheimer's Disease over 200 min are shown in Fig. 2a (compare right versus left).

2.4. Peak identification

Peak identification relied upon a database of relevant peaks [16] together with a priori frequency and baseline information. For every peak in the database, a frequency range was searched for a maximum and a baseline created by linear interpolation through flat regions of the spectra containing no ^{13}C peaks. The true peak heights were then used to estimate concentration of

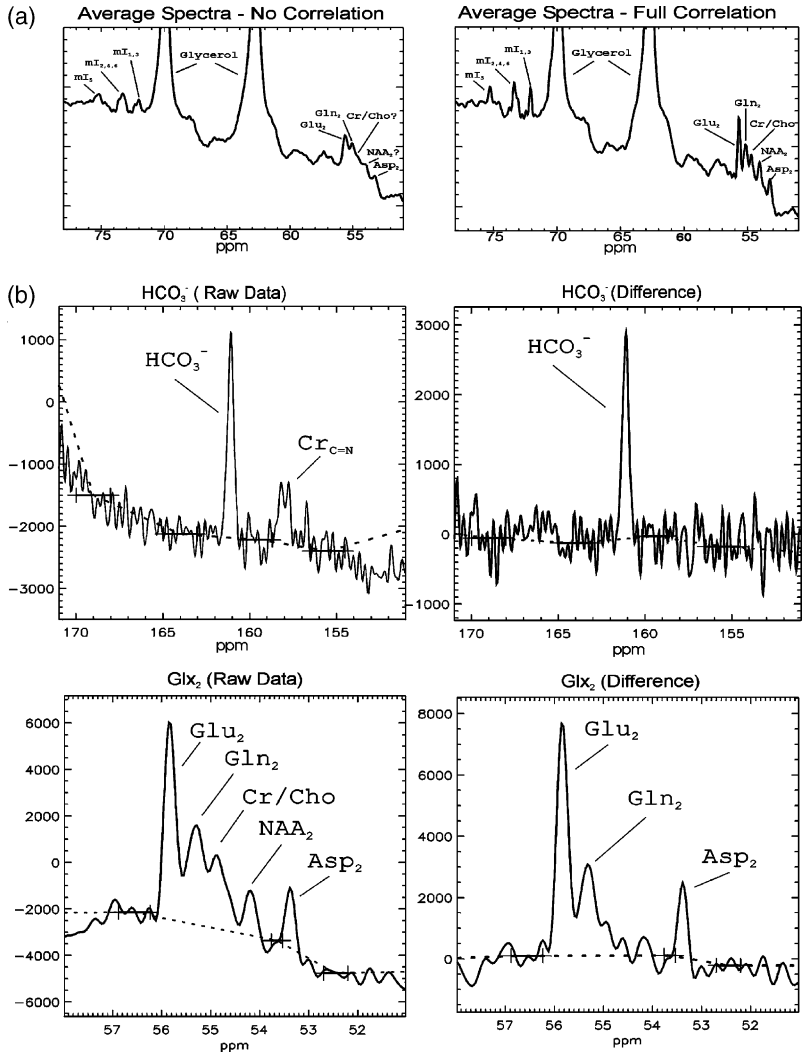

Fig. 2. Effects of automated data processing. (a) Averaging over 200 min in a patient with Alzheimer's Disease without (left) and with (right) automatic spectral correlation schemes. Note that in the uncorrected spectrum the myo-inositol peaks are extremely broad and the Cr/Cho and NAA_2 peaks are difficult to resolve. (Abbreviations: mI, myo-inositol; Glu_2, glutamate carbon 2; Gln, glutamine, Cr/Cho, co-resonating choline and creatine; NAA, *N*-acetyl aspartate; Asp2, aspartate carbon 2.) (b) Peak determination of raw data (left) and difference spectra (right) of a 20 min spectral block acquired 160 min after oral administration of both [1-^{13}C]acetate and [1-^{13}C]glucose in a control. The upper figures show enriched bicarbonate (HCO_3) and the C=N group of creatine; the lower figures show enriched [2-^{13}C]Glx (glutamate and glutamine), NAA_2, and Asp_2, as well as natural-abundance Cho/Cr. Scales are in arbitrary institutional units proportional to signal intensity. Both raw data and difference methods are used in the final data analysis (see text). (c) Comparison of difference spectra using a simulated baseline based on 5 min of baseline scanning (left) versus a real baseline based on 20 min of baseline scanning (right). Note that, by simulating the baseline, peaks representing non-enriching metabolites appear between Glu_2 and Asp_2 due to incomplete differencing. The use of a simulated baseline was required only occasionally. (d) Myo-insoitol signal determination by individual peaks (left) and by folding into a super pseudo-singlet (right). Both methods are applied to quantification of metabolites, with the average of the two providing the most reliable estimates see text).

the sum of the enrichment and natural abundance of metabolites (Fig. 2b, left) or enrichment alone from difference with natural abundance scans (Fig. 2b, right). The illustrative example is taken from a human subject who received simultaneous infusions of [1-^{13}C]glucose and [1-^{13}C]acetate, giving rise to HCO_3^- (Fig. 2b, upper panel) and ^{13}C-glutamate (Glu), glutamine (Gln), together referred to as Glx_2 (Fig. 2b, lower panel), as well as *N*-acetyl aspartate (NAA), creatine (Cr), choline (Cho), and aspartate (Asp).

Difference spectra were calculated by subtracting the sum of all non-enriched natural abundance spectra (Fig. 2c, right). This technique sufficed for 90% of all in vivo data sets. In the remainder, a simulated baseline calculated by passing a 15-point boxcar filter over the sum of available baseline spectra was used in subtraction (Fig. 2c, left).

Direct measurements of signal intensity (termed 'raw data' in Fig. 2b) characterized signal changes over time. Difference spectra were required to interpret the under-

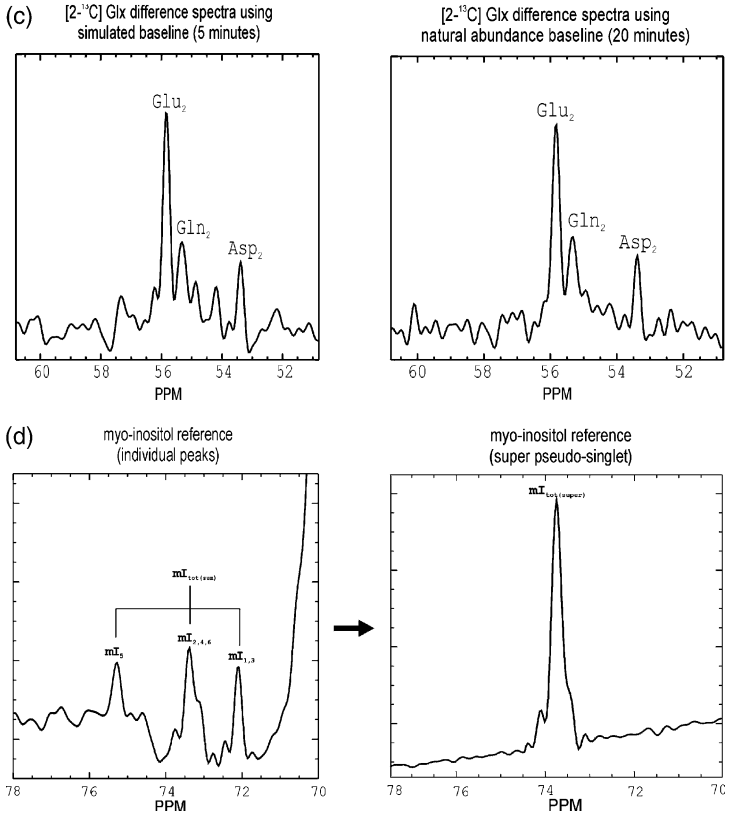

Fig. 2. (*continued*)

lying lipids or macromolecules. Both measurements were used.

2.4.1. Determination of concentration

Model solutions were used to calculate conversion factors from detected ^{13}C myo-inositol, yielding estimates for concentrations of labeled metabolites [10,15]. The concentration of myo-inositol was determined in each subject using ^{1}H MRS [18,19].

Two methods of quantifying the total myo-inositol signal were used:

1. The peak heights of each observable peak of myo-inositol were measured independently:

$$\mathrm{mI}_{\mathrm{tot(sum)}} = \mathrm{mI}_5 + \mathrm{mI}_{2,4,6} + \mathrm{mI}_{1,3}.$$

2. The regions containing myo-inositol peaks were broken into several segments and folded upon each other to yield a super pseudo-singlet with a peak height measurement of $\mathrm{mI}_{\mathrm{tot(super)}}$ (Fig. 2d).

Measurement of the myo-inositol signal $\mathrm{mI}_{\mathrm{tot(super)}}$ via the super pseudo-singlet tends to underestimate the true myo-inositol signal, whilst the independent peak measurement of $\mathrm{mI}_{\mathrm{tot(sum)}}$ tends to overestimate the actual peak. For these reasons, the final myo-inositol signal, S_{mI}, was determined by the average of these two methods (Table 1).

Given a metabolite A with concentration [A] and spectral signal intensity S_{A}; a reference signal of myo-inositol (mI) with concentration [mI], and signal intensity S_{mI}; and a conversion factor $C_{\mathrm{mI}\to\mathrm{A}}$, we compute the concentration [A] by assuming a natural abundance for the reference (0.011 for ^{13}C):

$$[\mathrm{A}] = \frac{S_{\mathrm{A}}[\mathrm{mI}]}{S_{\mathrm{mI}}} C_{\mathrm{mI}\to\mathrm{A}}(0.011),$$

$C_{\mathrm{mI}\to\mathrm{A}}$ values computed through model phantoms which were comparable to those used in [10], are shown in Table 2.

2.5. Assembly of enrichment time courses

The peak determinations were saved to files assembled through a program written in Perl and output as a summary table. Excel extended with the XLXtrFun toolkit [20] was used to read this file and to translate observed signal into concentrations via conversion factors. In addition, the following measurements and methods were employed:

(1) Peak measurements of myo-inositol: Averaging all spectra from a given study resulted in a highly reliable estimate for intrinsic myo-inositol signal.

(2) Averaging: In order to increase signal-to-noise (particularly for [1-^{13}C]acetate studies), spectra were assembled into 20-min blocks. The effects of averaging versus not averaging are shown in Fig. 2a.

Table 1
Impact of mI quantification methods and automated spectral correlation on ^{13}C metabolite ratios

Metabolite	Ratio of metabolite to mI_{sum}			Ratio of metabolite to mI_{super}			Ratio of metabolite to mI_{avg}		
	Correlation[a]		σ (%)[b]	Correlation[a]		σ (%)[b]	Correlation[a]		σ (%)[b]
	None	Full		None	Full		None	Full	
$Glc_{1\beta}$	1.38	1.56	13.5	2.36	2.08	−11.8	1.74	1.78	2.7
$Glc_{1\alpha}$	0.8	0.87	9.2	1.37	1.16	−15.2	1.01	0.99	−1.2
Glu_2	0.49	0.59	19.2	0.84	0.78	−7.4	0.62	0.67	7.8
HCO_3^-	0.14	0.17	20.9	0.23	0.23	−2.2	0.17	0.2	13.8

σ (%) is the percent difference between the values in a.

[a] Ratios of metabolites against myo-inositol for spectra processed without and with auto-correlation mechanisms are displayed.

[b] Small differences in ratio determination between broad (uncorrelated) and well-resolved (correlated) spectra are desirable, as this is an indication of robustness of measurement.

Table 2
Conversion factors for translating ^{13}C metabolite signal intensities to concentrations

Metabolite (A)	σ	$C_{mI\rightarrow A}$
Glu_5	182.0	10.16[a]
$NAA_{4,C=O}$	179.5	10.66
Gln_5	178.4	10.54
Glu_1	175.3	10.21
Gln_1	174.8	10.65
NAA_1	174.3	15.14
HCO_3^-	161.0	19.07
$Cr_{C=N}$	157.9	21.35
Glc_{1b}	96.8	9.42
Glc_1	93.0	14.36[a]
$Glc_{3,5\beta}$	76.8	4.94
mI_5	75.3	5.21
$mI_{2,4,6}$	73.3	2.48
mI_{13}	72.1	2.47
Glu_2	55.7	6.96
Gln_2	55.2	6.62
Cr_4	54.7	7.97
NAA_2	54.2	5.72
Asp_2	53.3	6.91[a]
NAA_3	40.4	6.78
Cr_3	37.8	14.26
Asp_3	37.5	8.81
Glu_4	34.4	7.84
Gln_4	31.8	7.67
Glu_3	27.9	7.55
Gln_3	27.2	7.76
Lac	21.0	10.16

[a] Values were experimentally determined from model solutions examined with the same ^{13}C MRS technique employed for human brain studies, and refer to the conversion factor, not to tissue concentration.

The use of peak heights was found to be more reliable than integrations (Table 3). The differences were further minimized when expressed as peak ratios to mI (Table 3) and, when time courses of ^{13}C enriched metabolites were examined (Fig. 3a and b).

(3) Final myo-inositol correction: The myo-inositol as estimated by the method described previously was used in order to make a final correction to all observed metabolites. A polynomial was fit to the myo-inositol signal and used to generate correction factors; one polynomial degree for every 30 min in the time course (Fig. 3c). The small but significant effects of this correction were seen only in the later phases of the time course of enrichment of [5-^{13}C]glutamine after infusion of [1-^{13}C]acetate as shown in Fig. 3d.

3. Results

In the first example the subject, a normal control received [1-^{13}C]glucose and [1-^{13}C]acetate simultaneously by mouth. In Fig. 4, the appearance of ^{13}C in each of the relevant, C1–C5 carbon atoms of glutamate and glutamine as well as the final oxidation product, HCO_3^-, confirms the predicted fates of ^{13}C glucose and ^{13}C acetate (see Discussion). The automated ^{13}C analytical technique also allows the detection of subtle metabolic changes, associated with the expected competition between glucose and acetate in glia (Fig. 5). Subjects are compared in whom [1-^{13}C]acetate alone, [1-^{13}C]glucose alone, or [1-^{13}C]acetate and [1-^{13}C]glucose in combination, were administered. The inhibitory effects of glucose entry on acetate metabolism are identified as reduction in HCO_3^-, [5-^{13}C]glutamate, and [5-^{13}C]glutamine, respectively. The earliest effect of this competition was observed in glutamate, possibly because of the larger pool size of glutamate in neurons.

In a clinical test of the automated analysis of ^{13}C data, ^{13}C MRS was performed in three epileptics on ketogenic diets and three normal controls, after [1-^{13}C]acetate infusion. ^{13}C incorporation into [5-^{13}C]Glu and [5-^{13}C]Gln was more prominent in patients than in controls; HCO_3^- on the other hand was unchanged (Fig. 6). The differences were statistically significant [24].

4. Discussion

The method of automated processing of ^{13}C data described has several advantages over previous manual technologies. Foremost is speed and accuracy, with ~95% time savings, and increased reproducibility; re-

Table 3
Effect of calculation of peak area versus estimation of peak height and peak-to-height ratios on quantitation of non-enriched ^{13}C metabolites

Metabolite and method of signal estimation	Metabolite mean signal intensity[a]	Metabolite signal intensity standard deviation	Percent standard deviation (%)	Ratio of metabolite mean signal to mean signal of mI
mI Integration	4508	684	15.2	
mI Height	7620	869	11.4	
$Cr_{C=N}$ Integration	822	334	40.6	0.182
$Cr_{C=N}$ Height	1366	232	17	0.179
$Glc_{3,5\beta}$ Integration	342	241	70.4	0.076
$Glc_{3,5\beta}$ Height	1038	331	31.9	0.136

[a] Signal intensities are in arbitrary institutional units. $Cr_{C=N}$, creatine; Glc, glucose.

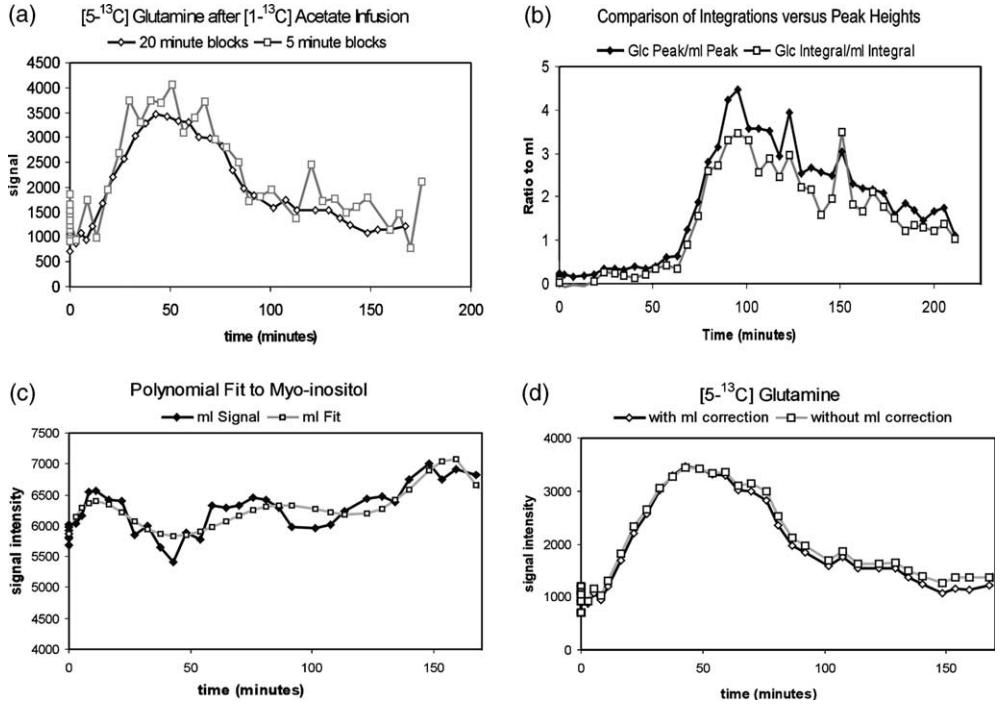

Fig. 3. Effects of automated data processing on time-courses of enrichment of ^{13}C metabolites. (a) [5-^{13}C]Glutamine after IV infusion of [1-^{13}C]acetate in a fed control. Note that the 20-min averaged time-course well approximates the time behavior of the 5-min averaged time-course, with considerable improvement in observed noise. (b) Comparison of integrations versus peak heights in the analysis of time courses for [1-^{13}C]glucose in human brain. (c) Polynomial fit to myo-inositol in order to characterize uncorrected changes in signal intensities. One polynomial order was used for every 30 min of experimental recording. The control shown above employs a 6th order polynomial and provides improved consistency in the determination of the mI reference signals. (d) The effects of polynomial myo-inositol correction on the time course of enrichment of [5-^{13}C]glutamine in a control who received [1-^{13}C]acetate intravenously. Note that the modifications to the time course are relatively slight, but become more pronounced towards the end of the time-course.

peated processing of the same data by different operators was highly reproducible. One possible source of error that primarily affects [3-^{13}C] and [4-^{13}C]glutamate and glutamine (Glx) is the incomplete subtraction of the methylenes of lipids during differencing. Differencing is required for Glx3 and Glx4, as the lipid signal is overwhelming (by up to a factor of 25 times) in comparison to the enriched metabolites. Over a short period of time, differencing works exceptionally well in removing the unwanted lipid signals and errors are slight. Over a long period of time (100+ min), however, these experimental changes can alter the intrinsic lineshape of metabolites, resulting in an artifact upon subtraction. The effect of these gradually advancing artifacts can be quite subtle. In Fig. 4, [3-^{13}C]glutamate appeared to enrich to a maximum concentration 25% greater than that of [2-^{13}C]glutamate. These preliminary findings are not statistically proven and require further analysis since it is generally accepted that [3-^{13}C]glutamate and [2-^{13}C]glutamate enrich symmetrically [7].

Another possible source of error is the use of the correction factors (Table 2) to establish metabolite concentration. Decoupling and the nuclear Overhauser effect (nOe) are essential but unknown contributions to the improved resolution and peak heights seen in vivo. However, despite efforts to ensure identical acquisition conditions, the use of in vitro model solutions may introduce errors if their relaxation, nOe, or decoupling

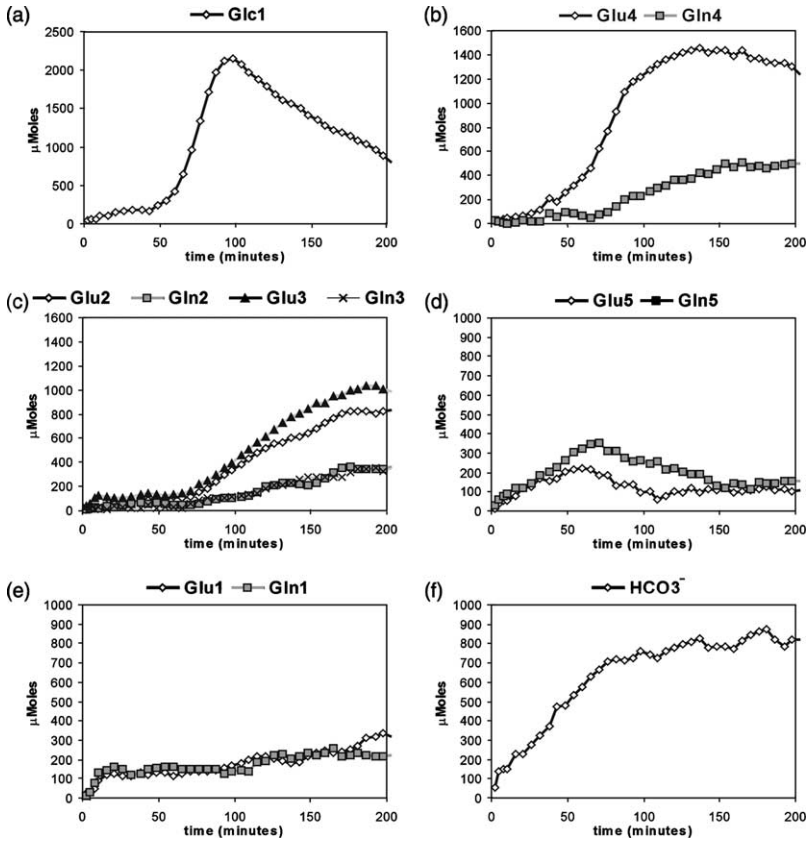

Fig. 4. Automated analysis of the time course of evolving ^{13}C isotopomers of glutamate in human brain. An example of the final time courses for ^{13}C metabolites measured via differencing to natural abundance is shown. The subject, an adult male, received both [1-^{13}C]glucose and [1-^{13}C]acetate by mouth before the ^{13}C examination. The precursor, [1-^{13}C]glucose appears in the brain before its metabolic products, C4 Glu, C2 Glu, and C3 Glu. The appearance of C5 Glu reflects glial metabolism of the second substrate, [1-^{13}C]acetate (not shown). The last glutamate isotopomer to appear, Glu C1, and the final oxidation product, HCO_3, arise from both of the precursors. This is a good example of in vivo isotopomer analysis: Gln, which is formed in glia by the metabolism of Glu, is seen later than Glu in carbons (C4, 2, and 3), which are enriched from the neuronal substrate glucose, while Gln5 which is formed from the glial substrate acetate, appears earlier than Glu5.

conditions differ greatly. We are currently examining the use of adaptive apodization as a means of reducing artifacts related to the lineshape variation induced by these differences. Lorentzian or LC Model fitting of peaks [22] could improve the reliability of spectral concentration determination at some considerable expense in reduced throughput, while extension of adjustable parameters in matching (e.g., apodization) could directly address inconsistencies due to failing homogeneity at some cost in resolution. However, LC Model relies equally heavily upon a priori hardware and system data acquired from model solutions in vitro. Elimination of these unknowns is the major advantage of scaling to intrinsic mI.

4.1. Practical applications

We have explored five different dynamic clinical NMR spectroscopy methods (intravenous and oral ^{13}C glucose, intravenous and oral [1-^{13}C]acetate, and a combined glucose plus acetate regime), all of which are described elsewhere in detail in [4,6,10,11]. In addition we have explored minor modifications in the dose and dietary state of patients [14]. In each case automated processing improved the results, examples of which are presented.

We demonstrate the value of independently identifying enrichment of each of the five carbons of both glutamate and glutamine, itself a variant of isotopomer analysis. Careful analysis of time-courses can add significantly to their diagnostic value.

Because non-steady-state is a 'fact-of-life' in many clinical ^{13}C examinations particularly of elderly patients with Alzheimer's Disease and of infants that cannot endure too prolonged an exam, DMA also features infrequently (for exceptions see [6,23]). Instead, we have found that ''pattern-recognition'' in difference spectra (DDS) is a powerful diagnostic tool that is applicable to non-steady state conditions and which is available after observer independent and reproducible data processing of infusion studies of the 60–100 min post-infusion duration.

Several examples are presented where the method of automated processing has illuminated subtle biochemical events in the human brain. In the first, improved resolution on intrinsic mI and enriched glutamate C_2 in a patient

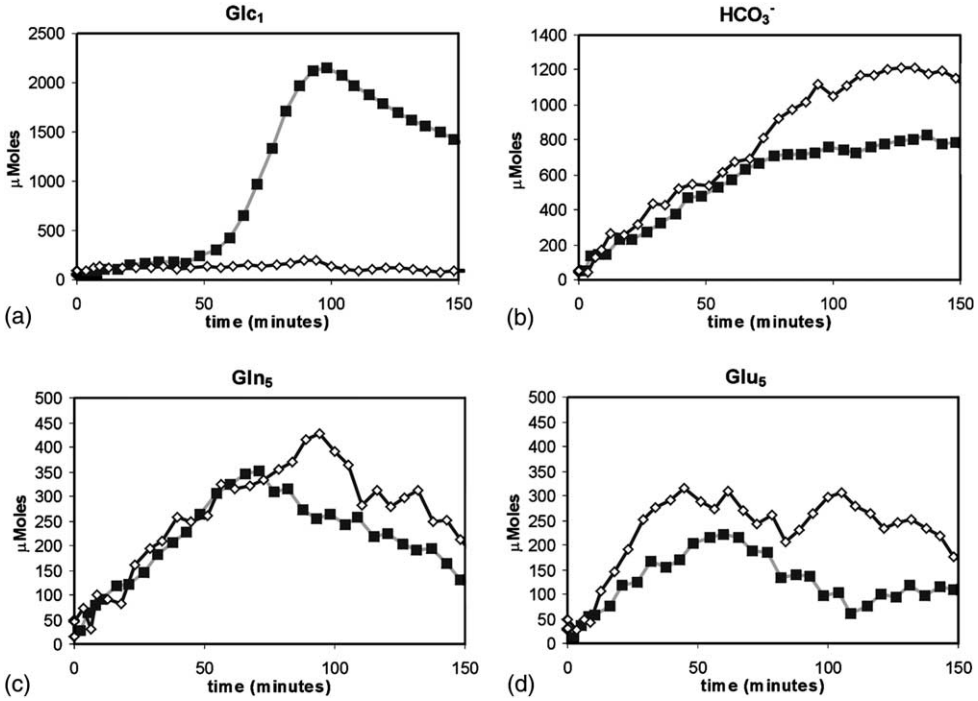

Fig. 5. Glial substrate competition in human brain in vivo. A comparison of the metabolic response of selected metabolites in an experiment where [1-^{13}C]acetate and [1-^{13}C]glucose were simultaneously administered (■) versus an experiment where only [1-^{13}C]acetate was administered (◇). Coincident with the maximum entry of ^{13}C glucose into the brain, glial glutamate, and glutamine formation from ^{13}C acetate, as well as HCO_3 formation are inhibited. This is an example of substrate competition in glial cells in vivo. The most noticeable effect of this competition was observed in glutamate, possibly because of the larger pool size of glutamatein neurons.

with Alzheimer's Disease (Fig. 3a) has permitted identification of significant abnormalities in the glutamate–glutamine cycle in this disorder [21]. ^{13}C MRS was used to follow the fates of [1-^{13}C]acetate and [1-^{13}C]glucose after their administration either individually or in combination. The rapid and specific enrichment of glutamate C5 and glutamine C5, indicative of exclusive glial metabolism of acetate, and of glutamate and glutamine C2 and C4 as well as aspartate C2 and C3, the products of neuronal metabolism of glucose, were observed with a time resolution of 5–10 min. The anticipated substrate competition between glucose and acetate in the normal human brain was clearly demonstrable (details in Figs. 5 and 6).

In epileptic patients treated by means of a ketogenic diet, incorporation of [1-^{13}C]acetate into glutamate and glutamine C5 was more prominent than in controls (details in [24], not shown) while incorporation into HCO_3^- was not significantly different. The results suggest abnormal glutamate–glutamine cycling in epileptic subjects on a ketogenic diet, compared to normal controls.

5. Conclusion

We present a technique for automated analysis of in vivo MR spectra of ^{13}C infusion data sets. This relies on straightforward correlation and conversion of spectral peak heights into concentrations. The methods presented here represent a simple but highly effective approach to preprocessing ^{13}C time course data for either direct examination or further modeling [9,10].

The data processing techniques presented here are concerned with correcting for variation across scanner and patient instabilities and the determination of a good first-order approximation for metabolic response, offering a practical method for clinical studies at the widely available field strength of 1.5 T. Subtle abnormalities of ^{13}C enrichment of the brain in small numbers of patients suffering from common or rare neurological disease states including Alzheimer's Disease [21], epilepsy [24], hepatic encephalopathy [10], mitochondrial encephalopathy, leukodystrophy, Canavan's disease [23], prematurity, hypoxic encephalopathy, and polyglucosan storage disease [25] have been identified by ^{13}C MR spectroscopy of the brain. The neurological significance of these abnormalities, often found in the presence of normal MRI remains to be established.

Access to this software, "Job Automation Utility for Yielding Advanced NMR Groupings," and accompanying user's manual, is available through our website at http://www.mrs-hmri.org/JAUYANG.

Acknowledgments

The work was supported by grants from Rudi Schulte Research Institutes (F.S.) and HMRI (B.R.). We are grateful to Alexander Lin, Else Danielsen, Kamini Patel,

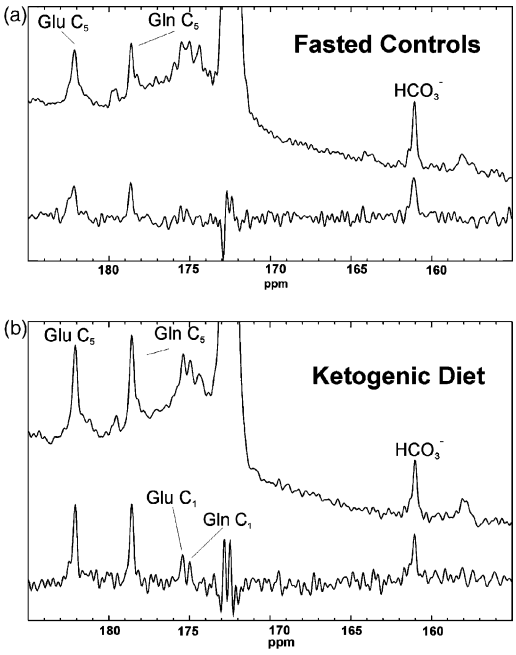

Fig. 6. Comparison of ^{13}C enrichments of human brain spectra of epileptics treated by ketogenic diet and normal controls. A commonly employed treatment for epilepsy is the feeding of a high-lipid diet which results in accumulation of ketone bodies in blood and brain and reduction in the frequency of seizures. The mechanism of this effect is unknown. To test the hypothesis that KD impairs glutamate neurotransmission, ^{13}C MRS studies were performed. Each subject received 10 g intravenous [1-^{13}C]acetate before ^{13}CMRS examination, and enrichments of C_5 Glx and HCO_3 were followed over 120 min. Summed spectra over the time period 60–90 min (above), as well as difference spectra (below) are illustrated for epileptic subjects on a ketogenic diet ($N = 2$) and normals ($N = 5$). The metabolic significance of these results is discussed in [24].

Cathleen Enriquez, and Teodora Beloreshka for contributions to this manuscript. The authors thank Drs. Stefan Bluml and Keiko Kanamori for helpful discussions. The authors also wish to dedicate this manuscript to the memory of John Jau-yang Shic.

References

[1] N. Beckmann, R. Fried, I. Turkalj, J. Seelig, U. Keller, G. Stalder, Non-invasive observation of hepatic glycogen formation in man by 13C MRS after oral and intravenous glucose administration, Magn. Reson. Med. 29 (1993) 583.

[2] G.F. Mason, R. Gruetter, D.L. Rothman, K.L. Behar, R.G. Shulman, E.J. Novotny, Simultaneous determination of the rates of the TCA cycle, glucose utilization, α-ketoglutarate/glutamate exchange, and glutamine synthesis in human brain by NMR, J. Cereb. Blood Flow Metab. 15 (1995) 12.

[3] I. Choi, I. Tkac, K. Ugurbil, R. Gruetter, Noninvasive measurement of [1-13C]glycogen concentrations and metabolism in rat brain in vivo, J. Neurochem. 73 (1999) 1300.

[4] S. Bluml, A. Moreno, J.-H. Hwang, B.D. Ross, [1-13C]glucose magnetic resonance spectroscopy of pediatric and adult brain disorders, NMR Biomed. 14 (2001) 19.

[5] D.L. Rothman, N.R. Sibson, F. Hyder, J. Shen, K.L. Behar, R.G. Shulman, In vivo nuclear magnetic resonsance spectroscopy studies of the relationship between the glutamate and glutamine neurotransmitter cycle and functional neuroenergetics, Philos. Trans. Roy. Soc. Lond. 354 (1999) 1165.

[6] S. Bluml, A. Moreno-Torres, F. Shic, C.-H. Nguy, B.D. Ross, Tricarboxylic acid cycle of glia in the in vivo human brain, NMR Biomed. 15 (2002) 1.

[7] R. Gruetter, E.R. Seaquist, K. Ugurbil, A mathematical model of compartmentalized neurotransmitter metabolism in the human brain, Am. J. Physiol. Endocrinol. Metab. 281 (2001) E100.

[8] P.J. Magistretti, L. Pellerin, D.L. Rothman, R.G. Shulman, Energy on demand, Science 283 (1999) 496.

[9] D.W. Choi, Glutamate neurotoxicity and disease of the nervous system, Neuron 1 (1988) 623.

[10] S. Bluml, A. Moreno-Torres, B.D. Ross, [1-13C]Glucose MRS in chronic hepatic encephalopathy in man, Magn. Reson. Med. 45 (2001) 981.

[11] F. Shic, B.D. Ross, K. Yahya, A. Lin, L. Lai, S. Bluml, A protocol for the synchronous assay of in vivo glial and neuronal metabolic rates in man, Proc. Int. Soc. Mag. Reson. Med. 1 (2002) 234, 10 Honolulu, Hawaii, USA.

[12] V. Lebon, P.F. Kitt, G.W. Cline, J. Shen, G.F. Mason, S. Dufour, K.L. Behar, G.I. Shulman, D.L. Rothman, Astroglial contribution to brain energy metabolism in humans revealed by 13C nuclear magnetic resonance spectroscopy: Elucidation of the dominant pathway for neurotransmitter glutamate repletion and measurement of astrocytic oxidative metabolism, J. Neurosci. 22 (2002) 1523.

[13] R.E. London, 13C Labelling in studies of metabolic regulation, Prog. NMR Spectrosc. 20 (1988) 337.

[14] A. Moreno, S. Bluml, J.-H. Hwang, B.D. Ross, Alternative [1-13C]glucose infusion protocols for clinical 13C MRS examinations of the brain, Magn. Reson. Med. 46 (2001) 36.

[15] S. Bluml, In vivo quantitation of cerebral metabolites concentration using natural abundance 13C MRS at 1.5 T, J. Magn. Reson. 136 (1999) 219.

[16] S. Bluml, J.-H. Hwang, A. Moreno, B.D. Ross, Novel peak assignments of in vivo 13C MRS in human brain at 1.5 T, J. Magn. Reson. 143 (2000) 292.

[17] W.H. Press, B.P. Flannery, S.A. Teukolsky, W.T. Vetterling, Numerical Recipes in C: The Art of Scientific Computing, Cambridge University Press, Cambridge, 1993.

[18] T. Ernst, R. Kreis, B.D. Ross, Absolute quantitation of water and metabolites in the human brain. I. Compartments and water, J. Magn. Reson. 102 (1993) 1.

[19] R. Kreis, T. Ernst, B.D. Ross, Absolute quantitation of water and metabolites in the human brain. Part II: Metabolite concentrations, J. Magn. Reson. 102 (1993) 9.

[20] S.A. Rauch, Advanced System Design and Development: XlXtrFun.xll(c). <http://www.netrax.net/~jdavita/XlXtrFun.htm> (1993–1999).

[21] A.P. Lin, F. Shic, C. Enriquez, B.D. Ross, Evidence of reduced glutamate neurotransmission in patients with Alzheimer's disease—An in vivo 13C MRS study, MAGMA (2003) 29.

[22] P.G. Henry, I. Tkac, R. Gruetter, Automatic quantitation of in vivo 13C spectra using LCModel, Proc. Int. Soc. Mag. Reson. Med. 1 (2002) 530, 10 Honolulu, Hawaii, USA.

[23] A. Moreno, B.D. Ross, S. Bluml, Direct determination of the *N*-acetyl-L-aspartate synthesis rate in the human brain by 13C MRS and [1-13C]glucose infusion, J. Neurochem. 77 (2001) 347.

[24] S. Bluml, F. Shic, L. Lai, K. Yahya, A. Lin, B.D. Ross, Glutamate–glutamine cycling in epileptic patients on ketogenic diets, Proc. Int. Soc. Mag. Reson. Med. 1 (2002) 417, 10, Honolulu, Hawaii, USA.

[25] F. Shic, L. Lai, A. Lin, K. Yahya, A. Moreno, S. Bluml, B.D. Ross, 13C Glucose magnetic resonance spectroscopy of neurodegenerative disorders, in: 8th International Conference of Alzheimer's Disease and Related Disorders, Stockholm, Sweden, vol., 2002.